

Validation of a model for an ionic electro-active polymer in the static case

M. Tixier¹ & J. Pouget²

¹ Laboratoire de Mathématiques de Versailles (LMV), UMR 8100, Université de Versailles Saint Quentin, 45, avenue des Etats-Unis, F-78035 Versailles, France

² Sorbonne Université, CNRS, Institut Jean le Rond d'Alembert, UMR 7190, F-75005 Paris, France

E-mail: mireille.tixier@uvsq.fr, pouget@lmm.jussieu.fr

April 2020

Abstract. IPMCs consist of a Nafion[®] ionic polymer film coated on both sides with a thin layer of metallic electrodes. The polymer completely dissociates when it is saturated with water, releasing small cations while anions remain bound to the polymer chains. When this strip is subject to an orthogonal electric field, the cations migrate towards the negative electrode, carrying water away by osmosis. This leads to the bending of the strip. We have previously published a modelling of this system based on the thermodynamics of irreversible processes. In this paper, we use this model to simulate numerically the bending of a strip. Since the amplitude of the deflection is large, we use a beam model in large displacements. In addition, the material permittivity may increase with ion concentration. We therefore test three permittivity models. We plot the profiles of the cations concentration, pressure, electric potential and induction, and we study the influence of the strip geometry on the tip displacement and on the blocking force. The results we obtain are in good agreement with the experimental data published in the literature. The variation of these quantities with the imposed electric potential allow us to discriminate between the three models.

Keywords : Electro-active polymers, Multiphysics coupling, Polymer mechanics, Nafion, EAP modelling, Ionic polymer, EAP beam

PACS numbers : PACS 47.10.ab, PACS 83.60.Np, PACS 82.47.Nj, PACS 77.65.-j

published in *Smart Materials and Structures* **29**(085019), 2020

<https://doi.org/10.1088/1361-665X/ab8fca>

1. Introduction

The present work proposes a study of a thin strip of electro-active polymer (EAP). More precisely, the study focuses on Ionic Polymer-Metal Composite (IPMC) belonging to the ionic class. We investigate responses of the EAP subject to an applied difference of electric potential on the metallic electrodes and an applied punctual force at the tip of the strip. In previous works we have constructed step by step a micro-mechanical model to establish the conservation laws for electro-active polymers (Tixier & Pouget 2014). Following this work, the constitutive equations were deduced from the hypothesis of local thermodynamics equilibrium and the Gibbs relation using the thermodynamics of irreversible processes (Tixier & Pouget 2016). The present study follows on from the spirit of the previous works and we want to characterize the behavior of a thin blade, especially the chemical, electrical and mechanical parameters under electro-mechanical loading.

The behavior of electro-chemical-mechanical interactions of EAP is of great interest for research and engineering advanced technology. Simply, we can say that an EAP is a polymer exhibiting a mechanical response, such a stretching, contracting or bending for example, when subject to an electric field. Conversely the EAP can produce electric energy in response to a mechanical load (Shahinpoor et al. 1998, Shahinpoor & Kim 2001, Bar-Cohen 2005, Pugal et al. 2010, Park et al. 2010). This particular property is highly attractive for applications. For instance, we can quote biomimetic devices (robotics, bio-inspired underwater robots such as fishes (Chen 2017), haptic actuators (artificial skin, tactile displays or artificial muscle (Deole et al. 2008, Matysek et al. 2009, Bar-Cohen 2005) and this material is an excellent candidate for energy harvesting (Farinholt et al. 2009, Tiwari et al. 2008, Aureli et al. 2010, Jean-Mistral et al. 2010, Cha et al. 2013). In addition promising applications to micro-mechanical systems (MEMS) at the sub-micron scale are also expected in medical engineering for accurate medical control or investigation, for instance Fang et al. (2007) and Chikhaoui et al. (2018).

Electro-active polymers can be categorized into two main groups depending on their activation mechanisms. The first one is electronic electro-active polymers and dielectrics which are subject to Coulomb force ; their volume change is due to the application of an electric field. For instance dielectric elastomers belongs to this category as well as piezoelectric and electrostrictive polymers. The second group of EAP is the ionic electro-active polymers. The latter are driven by the displacement of ions inside the material. The polyelectrolyte gels, ionic polymer-metal composites,

conductive polymers are such media. One of the advantages of the these polymers is that they can be activated by very low difference of electric potential of about 1 – 5 Volts. However, they can only be operated within electrolyte medium.

Most efforts have been devoted on electronic conducting polymers (E.C.P.) belonging to the ionic class in order to improve strain, output forces and response times. These polymers are used for multilayer polymer composite combined with a polymer which can be considered as ion reservoir to improve ion transfer. Trilayer actuators made of solid polymer electrolyte film sandwich between two electronic conducting polymers have been reported in Festin et al. (2014) and Nguyen et al. (2018). One of the advantage of these electro-active polymers is that they can operate in air and they are good candidates for biomimetic devices. Efforts have been conducted to increase the integrating biocompatible conducting polymers into continuum micro-robots. Developments of such biocompatible conducting polymers with the aim at designing accurate position control for the trajectory of the telescopic soft robots have been studied by Chikhaoui et al. (2018).

Modeling EAP is not an easy task, especially the model must include electro-mechanical and chemical-electric couplings of ion transport, electric field action and elastic deformation. Different kinds of approach have been proposed in the literature according to the underlying physics of chemical activation (Shahinpoor & Kim 2001, Brunetto et al. 2008, Deole et al. 2008, Bahramzadeh & Shahinpoor 2014). An instructive and comprehensive review paper devoted to IPMC has been proposed by Jo et al. (2013). The authors present the chemico-physical mechanisms involved in IPMCs. As a complement to the previous references, a set of interesting studies has been devoted to the modeling of EAP. Among them, Wallmersperger et al. (2009) develop a thermodynamically based mechanical model involving the chemico-electric transport phenomenon. Numerical simulations are proposed for a strip of EAP made of Nafion[®] 117 Li^+ . The authors deduce the profiles, within the strip thickness, of the electric charge density, electric potential, electric field and strain. Nardinocchi et al. (2011) deduce a model based on the 3-D theory of linear elasticity. The thermodynamics allows them to introduce chemo-electro-mechanical coupling and they deduce the constitutive equations of the material, especially a Nernst-Planck like equation is deduced. Their study continues with numerical illustrations for a thin strip of EAP. Moreover, time evolution at low frequency is proposed as well. It is noteworthy that these papers are partly, in their spirit, rather close to the present model. Nevertheless, their results

depend strongly on adjustable parameters to fit the experimental results. In their model, the Fourier law, Darcy law and the generalized rheological constitutive equation are not presented. Moreover, using their adjustable phenomenological parameters the authors deduce a dielectric permittivity greater than ours.

A continuum approach for multiphase materials has been investigated by Bluhm et al. (2016). The authors write down the conservation laws and the entropy inequality based on the theory of porous media for an arbitrary number of individual constituents. In spite of the rather thorough investigation, the authors do not compare their results with those proposed in the literature. However, their constitutive laws are related to the material constituents and not to the macroscopic medium, and their coefficient are not numerically evaluated.

The present model is mainly based on an averaging method of the microscopic description of phases in order to deduce the macroscopic behavior of the material. Thanks to this approach, the constitutive coefficients for the whole material are computed with the help of the microscopic physico-chemical properties of the constituents (volume fractions, mass densities, chemical potentials, electric charges, etc.) and physical meanings are identified.

An important polymer property that we would like to address is the dependency of the dielectric permittivity with the cation concentration in the polymer. As matter of fact, the dielectric constant of the polymer is not absolutely homogeneous within the strip thickness. Accordingly, it seems that the ionic transport when a difference of electric potential is applied to the polymer strongly modifies the dielectric constant along the thickness direction of the blade. This question will be examined and discussed in details in the forthcoming sections.

The paper is organized as follows: the next section is devoted to the description of the IPMC and chemico-physical process of activation is briefly described. This section reports also the way of modeling the EAP, especially, the conservation laws and constitutive equations are summarized. Section 3 focuses on the application of the model to a slender beam made of thin layer of EAP. A part of the section highlights the influence of the cation concentration within the thickness on the dielectric permittivity. Three kinds of dielectric laws will be considered. Numerical simulations are presented in Section 4. The profiles of the relevant variables and the scaling laws are reported. Comparisons to the experimental data available in the literature are discussed according to the chosen law of

the dielectric permittivity.

2. Modelling of the polymer

2.1. Description of the material and hypothesis

We study an IPMC (ionic polymer-metal composite): the system consists in an ionic electro-active polymer (EAP) blade of which the two faces are covered with thin metal layers acting as electrodes. The model we developed applies for example to Nafion[®], an ionic polymer well documented in the literature that we will use for the validation of our constitutive equations. When saturated with water, this polymer dissociates quasi completely, releasing small cations in water whereas anions remain bound to the polymer backbone (Chabe 2008). When a potential difference is applied between the two electrodes, the cations migrate towards the negative electrode, carrying the water away by osmosis. As a result, the blade contracts on the side of the positive electrode and swells on the opposite side, causing its bending (Figure 1).

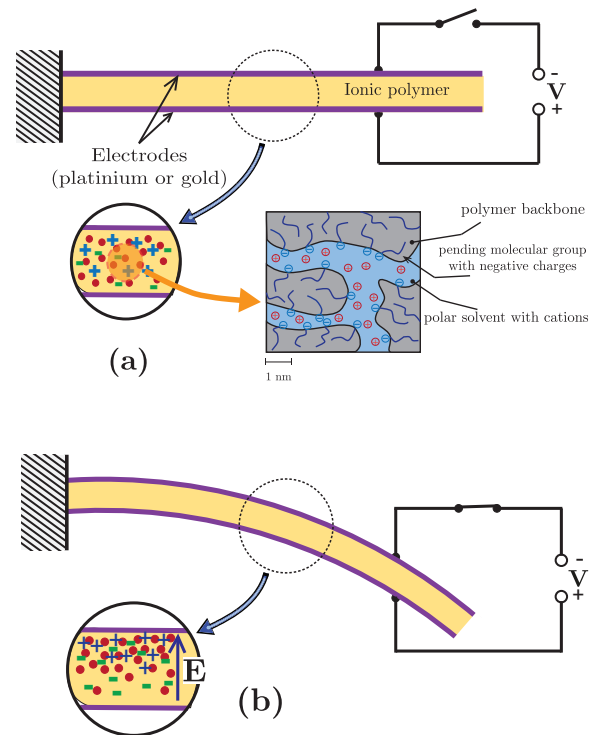


Figure 1. Deformable porous medium: (a) Undeformed strip (b) Strip bending under an applied electric field

To model the electro-active polymer, we used a "continuous medium" approach. Negatively charged polymer chains are assimilated to a deformable, homogeneous and isotropic porous medium in which flows an ionic solution (water and cations). The system is therefore composed of two phases and three

components which move relative to each other: the cations, the solvent (water) and the porous solid. The solid and liquid phases (water + cations) are separated by an interface without thickness. The three components are respectively identified by the subscripts 1, 2 and 3; 4 denotes the solution (1 + 2) and i the interfaces. Gravity and magnetic induction are supposed to be negligible; the only external force exerted is therefore the electric action. The different phases are supposed to be incompressible and the solution diluted. It is further recognized that solid deformations are small.

2.2. Basis of the model

We used a coarse-grained model developed for two-component mixtures (Ishii & Hibiki 2006). We define two scales. The conservation equations are first written at the microscopic level for each phase and for the interfaces. At this scale (typically about 100 Å), the elementary volume contains one phase only but is large enough so that the medium can be considered as continuous. The macroscopic equations of the material are deduced by averaging the microscopic ones using a presence function for each phase and interface. For each phase k and for the interfaces, a Heaviside-like function of presence is defined. The macroscale quantities are obtained by averaging the corresponding microscale quantities weighted by the functions of presence. This volume average is assumed to be equivalent to a statistical average (ergodic hypothesis). At the macroscopic scale, the representative elementary volume (R.E.V.) must be large enough so that these averages are relevant, but small enough so that the average quantities could be considered as local. According to Gierke et al. (1981) and Chabe (2008), its characteristic length is about 1 μm .

To write the balance equations, it is necessary to calculate the variations of the extensive quantities for a closed system in the thermodynamic sense. At the microscopic scale, we use the particle derivative or derivative following the motion of a constituent or an interface. At the macroscopic scale, the three constituents velocities are different; we introduce a "material derivative" or derivative following the movement of the three constituents $\frac{D}{Dt}$, which is a weighted average of the particle derivatives related to each constituent (Coussy 1995, Biot 1977).

2.3. Conservation laws

We thus obtain balance equations of mass (1), momentum (2), total, kinetic, potential and internal energy densities (3), entropy, electric charge (4) and

the Maxwell equations (5) for the complete material (Tixier & Pouget 2014)

$$\frac{\partial \rho}{\partial t} + \text{div}(\rho \vec{V}) = 0, \quad (1)$$

$$\rho \frac{D\vec{V}}{Dt} = \text{div} \underline{\underline{\sigma}} + \rho Z \vec{E}, \quad (2)$$

$$\begin{aligned} \rho \frac{D}{Dt} \left(\frac{U}{\rho} \right) &= \sum_{3,4} (\underline{\underline{\sigma}}_k : \text{grad} \vec{V}_k) \\ &+ \left(\vec{I} - \sum_{k=3,4,i} (\rho_k Z_k \vec{V}_k) \right) \cdot \vec{E} - \text{div} \vec{Q}, \end{aligned} \quad (3)$$

$$\text{div} \vec{I} + \frac{\partial \rho Z}{\partial t} = 0, \quad (4)$$

$$\text{rot} \vec{E} = \vec{0}, \quad \text{div} \vec{D} = \rho Z, \quad \vec{D} = \varepsilon \vec{E}, \quad (5)$$

where ρ_k denotes the densities relative to the volume of the whole material, \vec{V} the velocity, $\underline{\underline{\sigma}}$ the stress tensor, Z the electrical charge per unit of mass, \vec{E} the electric field, U the internal energy density, \vec{I} the current density vector, \vec{Q} the heat flux, \vec{D} the electrical induction and ε the dielectric permittivity. Subscripts refer to a phase, interface or a constituent and quantities without subscript are relative to the whole material.

We verify that the stress tensor of the whole material is symmetrical. The second member of equation (3) highlights the source terms of the internal energy (viscous dissipation and Joule heating) and its flux \vec{Q} . Equations (4) and (5) show that an EAP behaves like an isotropic homogeneous linear dielectric. In the last Maxwell equation, the permittivity of the whole material is obtained by a local mixing law, and is therefore likely to vary over space and time.

2.4. Constitutive equations

We make the hypothesis of local thermodynamic equilibrium. The Gibbs relation of the whole material is deduced from the Gibbs relations introduced by de Groot et Mazur (1962) for a deformable solid and for a two-constituent fluid

$$\begin{aligned} T \frac{d}{dt} \left(\frac{S}{\rho} \right) &= \frac{d}{dt} \left(\frac{U}{\rho} \right) + p \frac{d}{dt} \left(\frac{1}{\rho} \right) \\ &- \sum_{k=1,2,3} \mu_k \frac{d}{dt} \left(\frac{\rho_k}{\rho} \right) - \frac{1}{\rho} (p \underline{\underline{1}} + \underline{\underline{\sigma}}^e) : \text{grad} \vec{V}, \end{aligned} \quad (6)$$

where T is the absolute temperature, S the entropy density, p the pressure, μ_k the mass chemical potentials, $\underline{\underline{1}}$ the identity tensor and $\underline{\underline{\sigma}}^e$ the equilibrium stress tensor. $\frac{d}{dt}$ denotes the derivative following the barycentric velocity \vec{V} . At equilibrium, it is assumed

that the material satisfies Hooke's law and that the liquid phase is newtonian and stokesian.

By combining the balance equations of internal energy and entropy with the Gibbs relation, we deduced the entropy production of the system. The thermodynamics of linear irreversible processes makes then possible to identify the generalized forces and fluxes and to deduce the constitutive equations of the electro-active polymer. According to the Curie symmetry principle, a coupling between a force and a flux of different tensorial ranks is impossible because of the isotropy of the medium.

We thus obtained a Kelvin-Voigt type stress-strain relation (7) and generalized Fourier's, Darcy's (8) and Fick's laws (9). Given the orders of magnitude of the different physico-chemical parameters of the polymer (in particular, we admit that the solution is diluted), these equations can be written in the isothermal case on a first approximation (Tixier & Pouget 2016)

$$\underline{\sigma} = \lambda (\text{tr} \underline{\epsilon}) \underline{1} + 2G \underline{\epsilon} + \lambda_v (\text{tr} \dot{\underline{\epsilon}}) \underline{1} + 2\mu_v \dot{\underline{\epsilon}}, \quad (7)$$

$$\vec{V}_4 - \vec{V}_3 \simeq -\frac{K}{\eta_2 \phi_4} \left[\text{grad} p - (CF - \rho_2^0 Z_3) \vec{E} \right], \quad (8)$$

$$\vec{V}_1 = \vec{V}_2 \quad (9)$$

$$-\frac{D}{C} \left[\text{grad} C - \frac{Z_1 M_1 C}{RT} \vec{E} + \frac{C v_1}{RT} \left(1 - \frac{M_1 v_2}{M_2 v_1} \right) \text{grad} p \right],$$

where $\underline{\epsilon}$ denotes the strain tensor, λ the first Lamé constant, G the shear modulus, λ_v and μ_v the viscoelastic coefficients; η_2 is the dynamic viscosity of the solvent, ϕ_k the volume fractions, K the intrinsic permeability of the solid, C the cations molar concentration, $F = 96487 \text{ C mol}^{-1}$ the Faraday's constant, ρ_2^0 the mass density of the solvent, D the mass diffusion coefficient of the cations in the liquid phase, M_k the molar masses, v_k the partial molar volumes and $R = 8.31 \text{ J K}^{-1}$ the gaz constant.

The generalized Darcy's law models the motion of the solution compared with the solid phase. This movement is caused by the pressure forces, and also by the electric field, which reflects the electro-osmosis phenomenon. The third equation expresses the motion of cations by convection (\vec{V}_2), by mass diffusion, under the actions of the electric field and the pressure field; it can be identified with a Nernst-Planck equation (Lakshminarayanaiah 1969). An estimation of these different terms in the case of Nafion[®]Li⁺ shows that the pressure one is negligible.

3. Application of the model to a static cantilevered beam

3.1. Beam model on large displacements

To validate this model, we apply it to an EAP strip clamped at its end O under the action of a permanent

electric field (static case). The other end A is either free or subject to a shear force preventing its displacement (blocking force). Consider an EAP strip of length L , of width $2l$ and of thickness $2e$; we define a coordinate system $Oxyz$ such that the Ox axis is along the length, the Oy axis along its width and the Oz axis parallel to the imposed electric field (see figure 2). For all numerical applications, we choose the Nafion[®]Li⁺, an EAP well documented; in the nominal case, the dimensions of the strip are $L = 2 \text{ cm}$, $l = 2.5 \text{ mm}$ and $e = 100 \text{ } \mu\text{m}$ and it is subject to an electric potential difference $\varphi_0 = 1 \text{ V}$. Considering these values and the exerted forces, this is a two-dimensional (x, z) problem. The strip being thin and given the high values of the deflection, we used a beam model in large displacements.

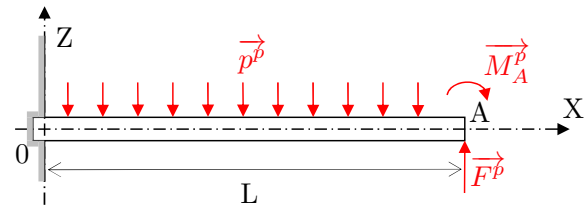


Figure 2. Forces exerted on the beam

The force system applied to the beam can be modelled by a distributed lineic force \vec{p}^b , a bending moment \vec{M}_A^b applied to the end A and in some cases a shear force \vec{F}^b in A. The strip being very slender, we venture the hypothesis that the distributed force is independent of the x coordinate along the beam and is orthogonal to it. The internal electrostatic forces of the strip cancel each other. The electric force produced by the electrodes also vanishes due to the electroneutrality condition. We deduce that the distributed force is zero everywhere.

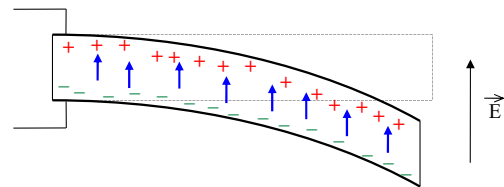


Figure 3. EAP bending strip

When a potential difference φ_0 is applied between the two faces, the cations and the solvent move towards the negative electrode, causing a volume variation and the bending of the strip (figure 3). The bending moment is therefore exerted along the Oy axis and results from the pressure forces $p = -\frac{\sigma_{xx}}{3}$

$$M_A^p = - \int_{-l}^l \int_{-e}^e \sigma_{xx} z \, dz \, dy = 6l \int_{-e}^e p z \, dz. \quad (10)$$

We made the usual hypotheses of a beam model: we assumed that the straight sections of the strip remain flat and normal to the neutral fibers after deformation (Bernoulli hypothesis) and that the stress and strain distributions are independent of the application points of the external forces (Barré Saint Venant hypothesis). We define a local coordinate system where \vec{t} and \vec{n} are the tangent and normal vectors; s and \bar{s} denote the curvilinear abscissas along the beam at the rest and deformed configurations respectively, \bar{n} the coordinate in the normal direction and θ the angle of rotation of a cross-section (figure 4). Let choose the point O as the origin of the curvilinear abscissas. No normal effort is applied, so we assumed that there is no beam elongation ($d\bar{s} = ds$).

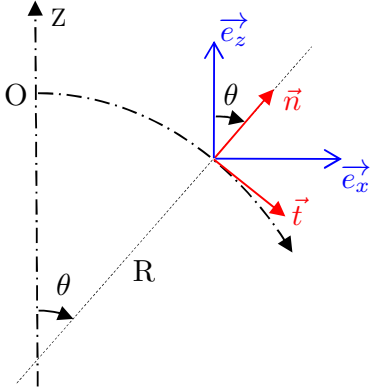


Figure 4. Beam on large displacements: coordinate system

The bending moment in the current section M^P and the radius of curvature R^P are

$$M^P = F^P (\bar{s} - L) + M_A^P, \quad \frac{1}{R^P} = \frac{d\theta}{d\bar{s}}. \quad (11)$$

Let \vec{u} the displacement vector; its gradient with respect to the reference configuration (beam at rest) is

$$\text{Grad } \vec{u} = \begin{pmatrix} (1 - \frac{\bar{n}}{R^P}) \cos \theta - 1 & -\sin \theta \\ (1 - \frac{\bar{n}}{R^P}) \sin \theta & \cos \theta - 1 \end{pmatrix}. \quad (12)$$

One deduces the strain tensor

$$\underline{\epsilon} = \frac{1}{2} [(\text{Grad } \vec{u} + \underline{1})^T (\text{Grad } \vec{u} + \underline{1}) - \underline{1}]. \quad (13)$$

The beam is thin, so $|\bar{n}| \ll R^P$ and

$$\epsilon_{xx} = -\frac{\bar{n}}{R^P} \left(1 - \frac{\bar{n}}{2R^P}\right) \simeq -\frac{\bar{n}}{R^P}. \quad (14)$$

In the case of a pure bending beam, the strain is $\epsilon_{xx} = \frac{M^P}{EI^P} \bar{n}$ using the constitutive law for the bending moment $M^P = \frac{EI^P}{R^P}$, where E is the Young's modulus and $I^P = \frac{4le^3}{3}$ the moment of inertia with respect to the Oy axis. The shear force has a negligible effect on the deflection, so we deduce

$$\frac{1}{R^P} = \frac{d\theta}{d\bar{s}} = \frac{F^P}{EI^P} (L - \bar{s}) - \frac{M_A^P}{EI^P}, \quad (15)$$

$$\theta = \frac{F^P}{2EI^P} \bar{s} (2L - \bar{s}) - \frac{M_A^P}{EI^P} \bar{s}. \quad (16)$$

The deflection w is obtained by integrating the relation $\frac{dz}{d\bar{s}} = \sin \theta$.

If $F^P = 0$, the beam is circle shaped (R^P is constant)

$$w = \frac{EI^P}{M_A^P} \left[\cos \left(\frac{M_A^P}{EI^P} L \right) - 1 \right], \quad \theta = -\frac{M_A^P}{EI^P} L. \quad (17)$$

It should be noted that this deflection calculation becomes incorrect if the angle of rotation exceeds 90° . With the hypothesis of small displacements, we would have obtained

$$w_s = -\frac{M_A^P}{2EI^P} L^2. \quad (18)$$

If a blocking force is exerted, the deflection is zero which provides on small displacements

$$F_s^P = \frac{3M_A^P}{2L}. \quad (19)$$

On large displacements, F^P verify

$$w = \int_0^L \sin \left[\frac{F^P}{2EI^P} x(x-2L) + \frac{M_A^P}{EI^P} x \right] dx = 0. \quad (20)$$

Let us compare this result with the calculation on small displacements. The above condition can be written

$$\begin{aligned} w = 0 &= \int_0^L \sin \left[\frac{1}{x^{*2}} (x + x_0)^2 - \frac{x^2}{x^{*2}} \right] dx \\ &= x^* \cos \left(\frac{x_0^2}{x^{*2}} \right) [S(x_1/x^*) - S(x_0/x^*)] \\ &\quad - x^* \sin \left(\frac{x_0^2}{x^{*2}} \right) [C(x_1/x^*) - C(x_0/x^*)], \end{aligned} \quad (21)$$

where

$$x^* = \sqrt{\frac{2EI^P}{F^P}}, \quad x_0 = \frac{M_A^P}{F^P} - L, \quad x_1 = \frac{M_A^P}{F^P}, \quad (22)$$

and where S and C denote the Fresnel functions

$$\begin{aligned} S(x) &= \int_0^x \sin t^2 dt = \sum_{n=0}^{+\infty} (-1)^n \frac{x^{4n+3}}{(2n+1)! (4n+3)}, \\ C(x) &= \int_0^x \cos s^2 dt = \sum_{n=0}^{+\infty} (-1)^n \frac{x^{4n+1}}{(2n)! (4n+1)}. \end{aligned} \quad (23)$$

In the case of Nafion[®] Li^+ , $E = 1,3 \cdot 10^8 \text{ Pa}$ (Bauer et al. 2005, Barclay Satterfield & Benziger 2009, Silberstein & Boyce 2010). Using the blocking force values provided by the literature in the nominal case (Newbury 2002, Newbury & Leo 2002, Newbury & Leo 2003), $\frac{x_0}{x^*} < \frac{x_1}{x^*} \sim 0.45$. We deduce, with a relative error around 2%

$$w \simeq \frac{F^P L^2}{6EI^P} \left(3 \frac{M_A^P}{F^P} - 2L \right) \simeq 0. \quad (24)$$

As a consequence, small displacements give a good approximation of the blocking force, that we will verify with our numerical simulations. On the contrary, the calculation of the deflection of the cantilevered beam requires a large displacements model.

3.2. Additional hypothesis and static equations for a bending strip

Let us evaluate the variations of the volume fraction of the solution ϕ_4 . Consider a small volume dV located at a distance z from the beam axis. According to Bernoulli's hypothesis, this volume takes the value $\frac{|R^p|+z}{|R^p|}dV$ when the beam bends with a radius of curvature R^p . The volume of the solid phase does not change, and the variation of liquid phase volume fraction is about

$$d\phi_4 = \frac{\phi_3 z}{|R^p|} = (1 - \phi_4) \frac{Mp}{EI^p} z \simeq (1 - \phi_4) \frac{2|w|}{L^2} z. \quad (25)$$

$\phi_4 \simeq 0.38$ (Cappadonia et al. 1994, Chabé 2008, Nemat-Nasser & Li 2000). In the nominal case, $w \sim 1$ mm (Nemat-Nasser 2002, Newbury & Leo 2002, Newbury 2002). ϕ_4 therefore varies less than 0.1% over the thickness of the beam. As a consequence, we assume that the volume fraction ϕ_4 is constant.

Considering the dimensions of the strip, we assume that the problem is two-dimensional in the Oxz plane. On a first approximation, we suppose that the electric field and induction are parallel to the Oz axis: $\vec{E} \simeq E_z \vec{e}_z$ and $\vec{D} \simeq D_z \vec{e}_z$. We further admit that C , E_z , D_z , p , ρZ and the electrical potential φ only depend on the variable z . Finally, we neglect the pressure term of the equation (9), an assumption that we will verify later. The equation system of our model then becomes

$$\begin{aligned} E_z &= -\frac{d\varphi}{dz}, & \frac{dD_z}{dz} &= \rho Z, \\ D_z &= \varepsilon E_z, & \rho Z &= \phi_4 F (C - C_{moy}), \\ \frac{dp}{dz} &= (CF - \rho_3^0 Z_3) E_z, & \frac{dC}{dz} &= \frac{FC}{RT} E_z, \end{aligned} \quad (26)$$

where

$$C_{moy} = -\frac{(1 - \phi_4) \rho_3^0 Z_3}{\phi_4 F}. \quad (27)$$

C_{moy} denotes the cations average concentration. The anions being attached to the polymer chains, they are uniformly distributed within the material; their concentration is therefore constant and equal to C_{moy} considering the electroneutrality condition. From Nemat-Nasser & Li (2000), the mass density of dry Nafion is $\rho_3^0 = 2 \cdot 10^3$ kg m⁻³, and its equivalent weight, that is the weight of polymer per mole of sulfonate groups, is $M_{eq} = 1.1$ kg eq⁻¹ (Chabé 2008, Colette 2008), which provides $Z_3 = -\frac{F}{M_{eq}} = -9 \cdot 10^{-4}$ C kg⁻¹. We deduce $C_{moy} = 3080$ mol m⁻³. We also choose an absolute temperature $T = 300$ K.

The boundary conditions and the electroneutrality condition are

$$\varphi(-e) = \varphi_0, \quad \varphi(e) = 0, \quad \int_{-e}^e \rho Z dz = 0. \quad (28)$$

According to (26), this last condition is equivalent to $D_z(e) = D_z(-e)$.

Table 1. Dielectric permittivity values

	ε^0 (Fm^{-1})	ε_{moy} (Fm^{-1})
constant	$5 \cdot 10^{-7}$	$5 \cdot 10^{-7}$
linear	0	10^{-4}
affine	$5 \cdot 10^{-7}$	10^{-4}

The permittivity strongly depends on the conductivity, hence of the electric charge; it increases with the water uptake (Deng & Mauritz 1992, Nemat-Nasser 2002), therefore with the cations concentration. We assume that it satisfies a mixing law

$$\varepsilon = \varepsilon^0 + \alpha C, \quad \text{with} \quad \alpha = \frac{\varepsilon_{moy} - \varepsilon^0}{C_{moy}}, \quad (29)$$

where ε_{moy} denotes the average permittivity of the material. We have considered three models of permittivity: constant, linear and affine. We choose our permittivity values in order that deflections and blocking forces are in agreement with the literature data, namely $0.5 < w < 1.5$ mm (Nemat-Nasser 2002, Newbury 2002) and $0.6 < F^p < 1.3$ mN (Newbury 2002, Newbury & Leo 2002, Newbury & Leo 2003) in the nominal case (table 1).

The Nafion relative permittivity found in the literature are very scattered, but compatible with those we have chosen. The average permittivity was measured by Deng & Mauritz (1992) for hydrated perfluorosulfonate ionomer membranes of the Nafion[®] family with different water contents. They obtained permittivity values between 10^{-7} F m⁻¹ and 10^{-6} F m⁻¹ by electrical impedance measurements. Nemat-Nasser (2002) deduced the permittivity of capacity measurements by assimilating the IPMC strip to a capacitor; for Nafion[®] 117 Li⁺, he got $\varepsilon \simeq 2.7 \cdot 10^{-3}$ F m⁻¹. Farinholt & Leo (2014) deduced a close value from their measurements but did not specify their method. Wang et al. (2014) measured the permittivity of Nafion[®] 117 Na⁺ by time domain dielectric spectroscopy. For samples obtained with different manufacturing methods and a water content about 22%, the permittivity ranges from $5 \cdot 10^{-5}$ to $5 \cdot 10^{-3}$.

3.3. Resolution with different permittivity models

Let us introduce dimensionless variables

$$\begin{aligned} \bar{E} &= \frac{E_z e}{\varphi_0}, & \bar{\varphi} &= \frac{\varphi}{\varphi_0}, & \bar{D} &= \frac{D_z}{e \phi_4 F C_{moy}}, \\ \bar{C} &= \frac{C}{C_{moy}}, & \bar{\rho Z} &= \frac{\rho Z}{\phi_4 F C_{moy}}, & \bar{p} &= \frac{p}{F \varphi_0 C_{moy}}, \\ \bar{z} &= \frac{z}{e}, & \bar{\varepsilon} &= \frac{\varepsilon \varphi_0}{e^2 \phi_4 F C_{moy}}. \end{aligned} \quad (30)$$

The system of equations and the boundary conditions

become

$$\begin{aligned}\bar{E} &= -\frac{d\bar{\varphi}}{d\bar{z}}, & \bar{D} &= \bar{\varepsilon}\bar{E}, \\ \frac{d\bar{D}}{d\bar{z}} &= \rho\bar{Z}, & \bar{\varepsilon} &= A_0\bar{C} + A_1, \\ \frac{d\bar{p}}{d\bar{z}} &= (\bar{C} + A_3)\bar{E}, & \frac{d\bar{C}}{d\bar{z}} &= A_2\bar{C}\bar{E}, \\ \rho\bar{Z} &= \bar{C} - 1, & \bar{D}(1) &= \bar{D}(-1), \\ \bar{\varphi}(-1) &= 1, & \bar{\varphi}(1) &= 0,\end{aligned}\quad (31)$$

with

$$\begin{aligned}A_0 &= \frac{\varphi_0(\varepsilon_{moy} - \varepsilon^0)}{e^2\phi_4FC_{moy}}, & A_1 &= \frac{\varphi_0\varepsilon^0}{e^2\phi_4FC_{moy}}, \\ A_2 &= \frac{F\varphi_0}{RT} \sim 38.7, & A_3 &= -\frac{\rho_2^0 Z_3}{C_{moy}F} \sim 0.303,\end{aligned}\quad (32)$$

in the nominal case. We deduce the following relations

$$\bar{C} = B_1 \exp(-A_2\bar{\varphi}), \quad (33)$$

$$\frac{\bar{D}^2}{2} = \frac{1}{A_2} \left(\frac{A_0}{2}\bar{C}^2 + (A_1 - A_0)\bar{C} \right) + A_1\bar{\varphi} + \frac{B_2}{2}, \quad (34)$$

$$\bar{p} = \frac{\bar{C}}{A_2} - A_3\bar{\varphi} + B_3, \quad (35)$$

where B_1 , B_2 and B_3 are three constants. The polymer strip behaves like a conductive material. The electric field, displacement and charge are then zero throughout the strip except near the sides. We can deduce

$$B_2 = \frac{1}{A_2}(A_0 - 2A_1 - 2A_1 \ln B_1). \quad (36)$$

The positive constant B_1 satisfies the electroneutrality condition (31)

$$A_0(1 + e^{-A_2})B_1^2 + 2(A_1 - A_0)B_1 - \frac{2A_1A_2}{1 - e^{-A_2}} = 0. \quad (37)$$

When $\varphi_0 \gtrsim 1$ V, $e^{-A_2} \ll 1$. In the case of a constant permittivity ($A_0 = 0$)

$$B_1 = \frac{A_2}{1 - e^{-A_2}} \simeq A_2. \quad (38)$$

In case of a linear permittivity ($A_1 = 0$)

$$B_1 = \frac{2}{1 + e^{-A_2}} \simeq 2, \quad (39)$$

and in the general case of an affine permittivity B_1 is of the order of 2

$$\begin{aligned}B_1 &= \frac{A_0 - A_1}{A_0(1 + e^{-A_2})} \left[1 + \sqrt{1 + \frac{2A_0A_1A_2}{(A_0 - A_1)^2} \frac{1 + e^{-A_2}}{1 - e^{-A_2}}} \right] \\ &\sim 2,\end{aligned}\quad (40)$$

assuming $A_1 \ll A_0$ and $\frac{2A_2A_1}{A_0} \ll 1$, assumption checked since we choose $\varepsilon^0 \ll \varepsilon_{moy}$. We moreover verify that B_1 tends toward 1 when φ_0 tends toward 0.

The system of equations (31) enable us to calculate the values of the various parameters at the center and at the boundaries of the strip (table 2). Note that \bar{p} is defined to within an additive constant.

Table 2. Center and boundary values of the different quantities

	-1	center	1
\bar{C}	$B_1 \exp(-A_2)$	1	B_1
$\rho\bar{Z}$	$B_1 \exp(-A_2) - 1$	0	$B_1 - 1$
$\bar{\varphi}$	1	$\frac{\ln B_1}{A_2}$	0
\bar{D}	$\bar{D}(1)$	0	$\bar{D}(1)$
$\bar{\varepsilon}$	A_1	$A_0 + A_1$	$A_0B_1 + A_1$
$\bar{p} - B_3$	$\frac{B_1 \exp(-A_2)}{A_2} - A_3$	$\frac{1}{A_2} - \frac{A_3 \ln B_1}{A_2}$	$\frac{B_1}{A_2}$

where $\bar{D}(1) = \sqrt{\frac{1}{A_2} [A_0 + 2A_1(A_2 - 1 - \ln B_1)]}$

The bending moment is given by

$$M_A^p = A_5 \bar{M} = A_5 \int_{-1}^1 \left(\frac{\bar{C}}{A_2} - A_3\bar{\varphi} \right) \bar{z} d\bar{z},$$

$$\text{with } \bar{M} = \int_{-1}^1 \bar{p} \bar{z} d\bar{z}, \quad (41)$$

$$A_5 = 6le^2F\varphi_0C_{moy},$$

$$\int_{-1}^1 \bar{C} \bar{z} d\bar{z} = 2\bar{D}(1) - \frac{A_0}{A_2}B_1 - A_1.$$

$I_\varphi = \int_{-1}^1 \bar{\varphi} \bar{z} d\bar{z}$ must be numerically evaluated. We deduce w , w_s , F^p , F_s^p and θ using (17) to (20).

The resolution of the equation system is tricky from a numerical point of view because of the steepness of the functions near the boundaries. We used different methods according to the permittivity model to obtain the best precision.

In the case of a constant permittivity ($A_0 = 0$), we use the variable $y = \ln \bar{C}$ which verifies

$$\begin{aligned}\frac{d^2y}{d\bar{z}^2} &= \frac{A_2}{A_1}(e^y - 1), \\ \frac{dy}{d\bar{z}} \Big|_1 &\simeq \frac{dy}{d\bar{z}} \Big|_{-1} = \sqrt{2\frac{A_2}{A_1}(A_2 - \ln A_2 - 1)},\end{aligned}\quad (42)$$

$$I_\varphi = \int_{-1}^1 \bar{\varphi} \bar{z} d\bar{z} = -\frac{1}{A_2} \int_{-1}^1 y \bar{z} d\bar{z}.$$

This differential equation can be numerically integrated near the boundaries, but not over the entire thickness.

In the case of a linear permittivity ($A_1 = 0$), the cation concentration can be calculated using the following differential equation

$$\frac{d^2\bar{C}}{d\bar{z}^2} = \frac{1}{\bar{z}_0^2} (\bar{C} - 1), \quad (43)$$

where $\bar{z}_0 = \sqrt{\frac{A_0}{A_2}} \ll 1$, which provides

$$\bar{C} = 1 + (B_1 - 1) \frac{\sinh(\bar{z}/\bar{z}_0)}{\sinh(1/\bar{z}_0)}. \quad (44)$$

The functions thus obtained are especially steep near the boundaries in this case, which makes the calculation of I_φ very delicate; we calculate the piecewise integral using Taylor expansions on some intervals.

In the case of an affine permittivity, the following equation can be numerically integrated over the entire interval

$$\frac{d^2 \bar{D}}{d\bar{z}^2} = \frac{A_2 \left(1 + \frac{d\bar{D}}{d\bar{z}}\right)}{A_0 \left(1 + \frac{d\bar{D}}{d\bar{z}}\right) + A_1} \bar{D}. \quad (45)$$

4. Simulation results

4.1. Hypothesis validation

The dimensionless equation (9) provides

$$\frac{d\bar{C}}{d\bar{z}} = A_2 \bar{C} \bar{E} [1 + A_4 (\bar{C} + A_3)], \quad (46)$$

where (Tixier & Pouget 2016)

$$A_4 = C_{moy} v_1 \left(1 - \frac{M_1 v_2}{M_2 v_1}\right) \simeq \frac{C_{moy}^2 M_1 M_2}{\rho_2^{02}} \simeq 1.2 \cdot 10^{-3},$$

($M_1 = 6.9 \text{ g mol}^{-1}$ and $M_2 = 18 \text{ g mol}^{-1}$ for Nafion[®]Li⁺). $A_4 (\bar{C} + A_3)$ corresponds to the pressure term; its maximum value (about 0.04) is reached near the negative electrode in the case of a constant permittivity, and it is of the order of $A_4 \ll 1$ in the center of the strip. We can therefore neglect the pressure term for the calculation of the bending moment.

For each of our simulations, we calculated the different parameters in small and large displacements. The difference between blocking forces calculated in small and large displacements is less than 1% in all simulations and largely below 0.1% as soon as the thickness exceeds $50 \mu\text{m}$. Small displacements are thus sufficiently accurate for the blocking force calculation. Concerning the deflection, the difference between both models is less than 1% when the deflection is less than 3.5 mm ; it otherwise becomes very large (over 100% sometimes, especially for low thicknesses). The large displacements model is thereby essential for the deflection evaluation. Moreover, we can verify that the small displacements calculation is an upper bound on deflection.

4.2. Profiles of different quantities

We have plotted the profiles of the various quantities in the thickness of the strip in the nominal case described in section 3 (Nafion[®]Li⁺ with $L = 2 \text{ cm}$, $l = 2.5 \text{ mm}$, $e = 100 \mu\text{m}$ and $\varphi_0 = 1 \text{ V}$). The profiles of dimensionless concentration, electric potential and displacement and pressure have similar aspects: the curves are almost constant in the central zone and very steep near the boundaries (figures 5 to 8).

The cation concentration profiles displays near the positive electrode a zone almost free of cations whose size depends on the permittivity model: $0.08 \mu\text{m}$ in

the constant case and $0.03 \mu\text{m}$ in the affine one. The linear model predicts a permittivity tending towards 0 and is therefore incorrect in this range. Near the negative electrode, there is an accumulation of cations over a characteristic length depending on the chosen permittivity model: close to $0.1 \mu\text{m}$ for a constant permittivity and $1 \mu\text{m}$ in linear and affine cases. The concentration on the negative electrode is twenty times higher with the constant permittivity model than in the two other cases. Nemat-Nasser (2002), Wallmersperger et al. (2009) and Nardinocchi et al. (2011) obtained a similar profile, although less steep.

The electric potential profiles look similar to those obtained by Wallmersperger et al. (2009) and Nardinocchi et al. (2011), although they are less steep in the vicinity of the electrodes. The linear and affine models give almost identical results for the other profiles. The constant model distinguishes by its steepness near the boundaries, with a characteristic length close to $0.02 \mu\text{m}$ near the negative electrode, twenty times smaller than the other models; near the positive electrode, its characteristic length is $0.1 \mu\text{m}$, five times larger than the other models for electric potential and pressure profiles. All three models provide nearly identical electrical displacement profiles with close boundary values. The pressure profiles are also very similar, except near the negative electrode where the constant model provides a boundary twenty times higher than the other two.

We furthermore verify that the electrical displacement is null in the central part of the strip with the three models, which confirms that the material behaves like a conductor.

4.3. Expected scaling laws

Let us determine the dependence of the mechanical quantities with respect to l , L , e and φ_0 . These quantities are written

$$\begin{aligned} M_A^p &= 6FC_{moy} l e^2 \varphi_0 \bar{M}, \\ \theta &= -\frac{9}{2} \frac{FC_{moy}}{E} \frac{L}{e} \varphi_0 \bar{M}, \\ F^p &= 9FC_{moy} \frac{l e^2}{L} \varphi_0 \bar{M}, \\ w_s &= -\frac{9}{4} \frac{FC_{moy}}{E} \frac{L^2}{e} \varphi_0 \bar{M}, \\ w &= \frac{2}{9} \frac{E}{FC_{moy}} \frac{e}{\varphi_0} \frac{1}{\bar{M}} \left[\cos \left(\frac{9}{2} \frac{FC_{moy}}{E} \frac{L}{e} \varphi_0 \bar{M} \right) - 1 \right], \end{aligned} \quad (47)$$

where F is a constant. $\bar{M} = \int_{-1}^1 \left(\frac{\bar{C}}{A_2} - A_3 \bar{\varphi} \right) \bar{z} d\bar{z}$ is a function of the constants A_0 , A_1 , A_2 , A_3 et B_1 . Let

$$A_0 = a_0 \frac{\varphi_0}{e^2}, \quad A_1 = a_1 \frac{\varphi_0}{e^2}, \quad A_2 = a_2 \varphi_0. \quad (48)$$

a_0 , a_1 , a_2 and A_3 like C_{moy} and E only depend on the chosen material.

Let us first look at the case where $\varphi_0 \gtrsim 1$; B_1 checks the approximate equation (see eq. (37))

$$a_0 B_1 (B_1 - 2) = 2a_1 (a_2 \varphi_0 - B_1), \quad (49)$$

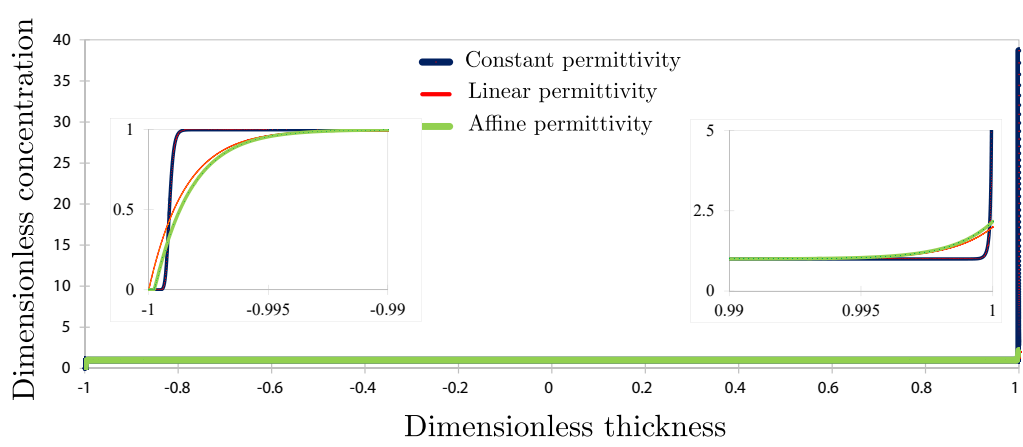


Figure 5. Variation of the dimensionless cation concentration in the thickness of the strip; the distribution close to the boundaries are detailed in insets. The constant permittivity model is in blue, the linear one in red and the affine one in green.

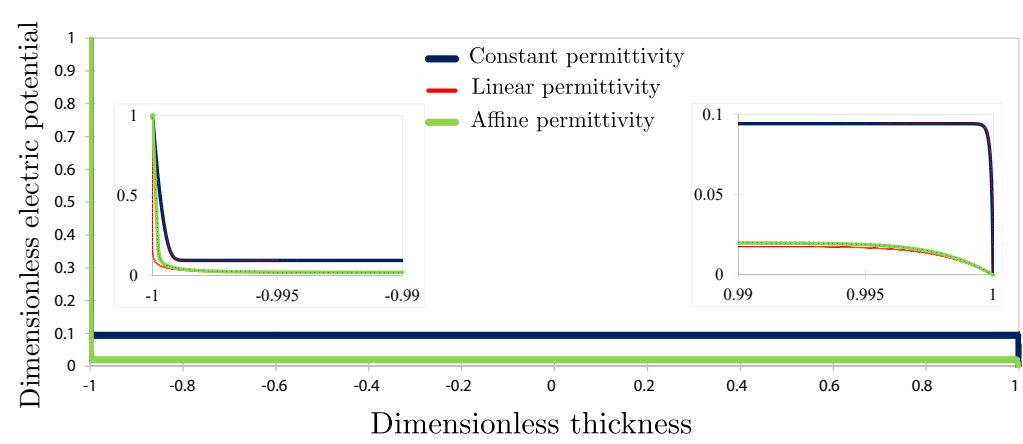


Figure 6. Variation of the dimensionless electric potential in the thickness of the strip; the distribution close to the boundaries are detailed in insets (same colours as in figure 5).

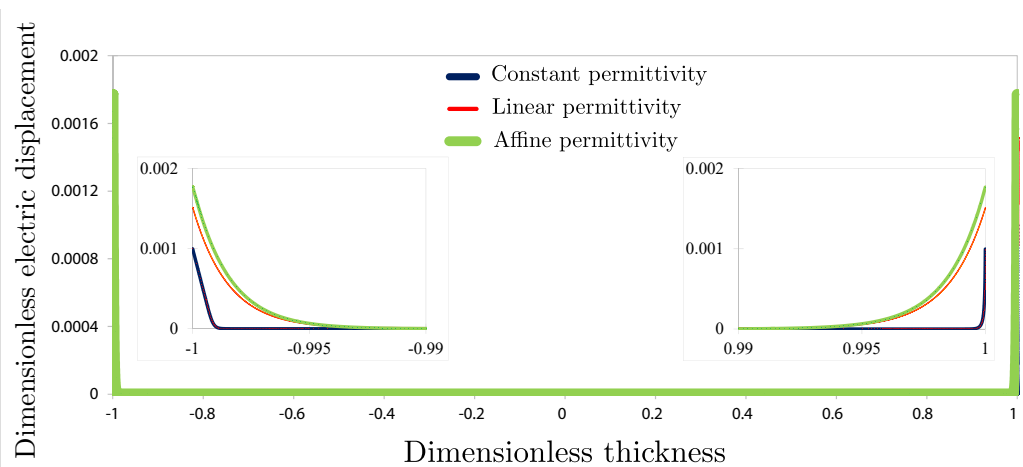


Figure 7. Variation of the dimensionless electric displacement in the thickness of the strip; the distribution close to the boundaries are detailed in insets (same colours as in figure 5).

and therefore depends only on φ_0 and the material. The pressure profile is almost constant throughout

the center of the strip and is very steep near the boundaries. It can be modelled by a constant between

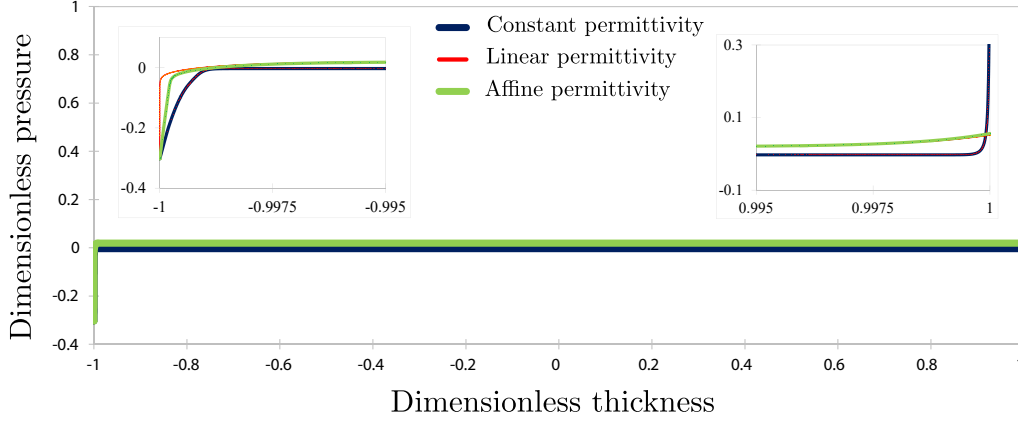


Figure 8. Variation of the dimensionless pressure in the thickness of the strip; the distribution close to the boundaries are detailed in insets (same colours as in figure 5).

two values $-\bar{z}_1$ and \bar{z}_2 with $\bar{z}_1, \bar{z}_2 \lesssim 0.99$. Assuming for example $0 < \bar{z}_1 < \bar{z}_2$

$$\bar{M} = \int_{-1}^{-\bar{z}_1} \bar{p} \bar{z} d\bar{z} + \int_{-\bar{z}_1}^{\bar{z}_2} \bar{p} \bar{z} d\bar{z} + \int_{\bar{z}_2}^1 \bar{p} \bar{z} d\bar{z}. \quad (50)$$

Given the low values of $\delta_1 = 1 - \bar{z}_1$ and $\delta_2 = 1 - \bar{z}_2$, we can expand in Taylor series up to the second order the first and last integrals

$$\begin{aligned} \int_{-1}^{-\bar{z}_1} \bar{p} \bar{z} d\bar{z} &= -\bar{p}(-1)\delta_1 + o(\delta_1^2), \\ \int_{-\bar{z}_1}^{\bar{z}_2} \bar{p} \bar{z} d\bar{z} &= 0, \\ \int_{\bar{z}_2}^1 \bar{p} \bar{z} d\bar{z} &= \frac{\bar{p}(0)}{2} (\bar{z}_2^2 - \bar{z}_1^2), \\ \int_{\bar{z}_2}^1 \bar{p} \bar{z} d\bar{z} &= \bar{p}(1)\delta_2 + o(\delta_2^2). \end{aligned} \quad (51)$$

Hence, in all cases and at the first order in δ

$$\bar{M} = A_3\delta_1 + \frac{B_1}{A_2}\delta_2 + \frac{1}{A_2}(1 - A_3 \ln B_1)(\delta_1 - \delta_2). \quad (52)$$

δ_1 and δ_2 can be roughly evaluated using the following formulas (thanks to eq. (31))

$$\left. \frac{d\bar{p}}{d\bar{z}} \right|_{-1} \sim \frac{\bar{p}(-\bar{z}_1) - \bar{p}(-1)}{\delta_1}, \quad \left. \frac{d\bar{p}}{d\bar{z}} \right|_1 \sim \frac{\bar{p}(1) - \bar{p}(\bar{z}_2)}{\delta_2}. \quad (53)$$

\bar{M} is therefore independent of L and l and approximately inversely proportional to e . Its dependence on φ_0 is more complex and linked with the chosen permittivity model. Given the values of a_0, a_1, a_2, A_3 and B_1 in the nominal case, we obtain with a precision of about 20%

$$\begin{aligned} \text{Constant case} \quad \bar{M} &\simeq \sqrt{\frac{a_1}{2}} a_3 \frac{\sqrt{\varphi_0}}{e}, \\ \text{Linear case} \quad \bar{M} &\simeq \sqrt{\frac{a_0}{a_2^2}} \frac{1}{e\varphi_0}, \\ \text{Affine case} \quad \bar{M} &\simeq \sqrt{\frac{a_0}{a_2^2}} \frac{f(\varphi_0)}{e\varphi_0}, \end{aligned} \quad (54)$$

$$\text{with} \quad f(\varphi_0) = \frac{\frac{a_1}{a_0} a_2^2 a_3 \varphi_0^2 + 2 \frac{a_1}{a_0} a_2 \varphi_0 + 1}{\sqrt{1 + 2 \frac{a_1}{a_0} a_2 \varphi_0}}.$$

We deduce the scaling laws presented in table 3.

Table 3. Expected scaling laws

	L	l	e	φ_0 constant	φ_0 linear	φ_0 affine
M_A^p	-	l	e	$\varphi_0^{3/2}$	-	$f(\varphi_0)$
θ	L	-	e^{-2}	$\varphi_0^{3/2}$	-	$f(\varphi_0)$
F^p	L^{-1}	l	e	$\varphi_0^{3/2}$	-	$f(\varphi_0)$
w_s	L^2	-	e^{-2}	$\varphi_0^{3/2}$	-	$f(\varphi_0)$

When the imposed electric potential is very small, B_1 tends to 1 for all permittivity models, C tends to C_{moy} and φ to φ_0 over the entire thickness of the strip. We check that all the mechanical quantities become null, which is in agreement with the experimental results.

4.4. Influence of the strip geometry

Our numerical simulations ascertain the results of the previous section with an excellent correlation: for the three permittivity models, the bending moment varies linearly with the width and thickness of the strip and is independent of its length.

The blocking force is proportional to the width and inversely proportional to the length, which is in good agreement with the results of Newbury & Leo (2003). It is also proportional to the thickness.

The predictions of the previous section are also well fitted by the deflection in large displacements; it is independent of the width and approximately proportional to L^2 : according to the chosen permittivity model, the power law that best approximates our simulations has an exponent between 1.90 and 1.96, and the variations of the ratio w/L^2 are less than 15% in all cases (figure 9). This is consistent with the results of Shahinpoor (1999). It varies almost like e^{-2} : we

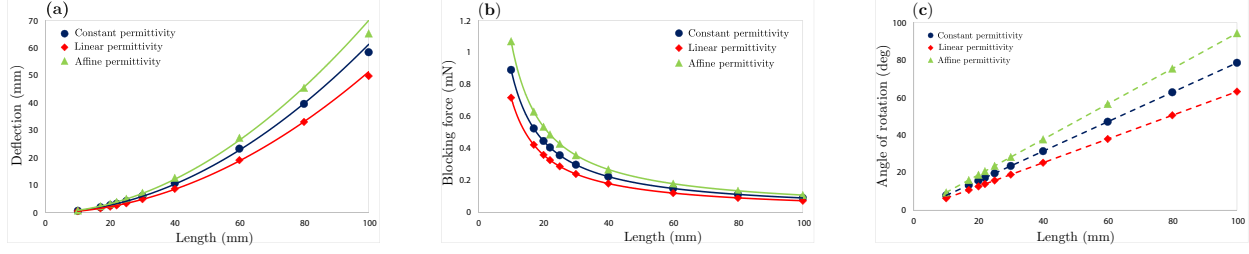


Figure 9. Influence of the length: (a) on the deflection; (b) on the blocking force; (c) on the angle of rotation. The constant permittivity model is in blue disks, the linear one in red diamonds and the affine one in green triangles. Fitting by power laws (solid curves) or linear law (dashed curves).

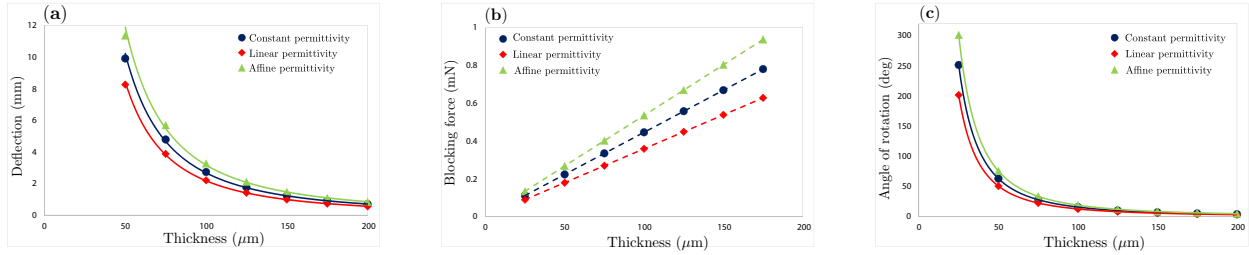


Figure 10. Influence of the thickness: (a) on the deflection; (b) on the blocking force; (c) on the angle of rotation (same colours, marks and curves as in figure 9).

find an exponent between -1.90 and -1.96 according to the chosen permittivity model and the variations of the product $w\epsilon^2$ are less than 14% (figure 10). This result is corroborated by the measurements of He et al. (2011) as well as by the simulations of Vokoun et al. (2015).

We also observe that the charge of the negative electrode $FC(e) = FB_1C_{moy}$ is independent of the thickness e with the three permittivity models, which agrees with the results obtained by Lin et al. (2012) for a close material.

4.5. Influence of the imposed electric potential

Unlike scaling laws, the relation between the different mechanical quantities and φ_0 depends on the chosen permittivity model. According to equations (47), the angle of rotation, the blocking force, the deflection in small displacements and the bending moment vary over the imposed potential in the same way. First, we check that the bending moment tends to 0 when φ_0 tends to 0 in all three cases using Taylor expansions. For imposed potentials close to 1 V, we have seen that M_A^p is proportional to $\varphi_0^{3/2}$ in the case of a constant permittivity, is almost constant if the permittivity is linear and is a complex function $f(\varphi_0)$ in the case of an affine permittivity (table 3, figure 11).

Bakhtiarpour et al. (2016) observed experimen-

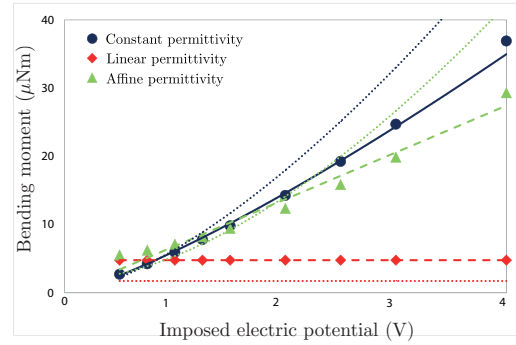


Figure 11. Influence of the electric potential on the bending moment: fitting by power law (solid curve), affine laws (dashed curves) and with equations (54) (dotted curves); same colours and marks as in figure 9.

tally an approximately linear relation between the deflection and the potential for actuators, and Shahinpoor et al. (1998) and Mojjarrad & Shahinpoor (1997) did the same for the sensor effect. Our simulations show a quite good correlation with a linear law if the permittivity is constant (the variation of the ratio w/φ_0 is about 30%); on the contrary, the results obtained with the other two models of permittivity do not agree with these experimental results. More pre-

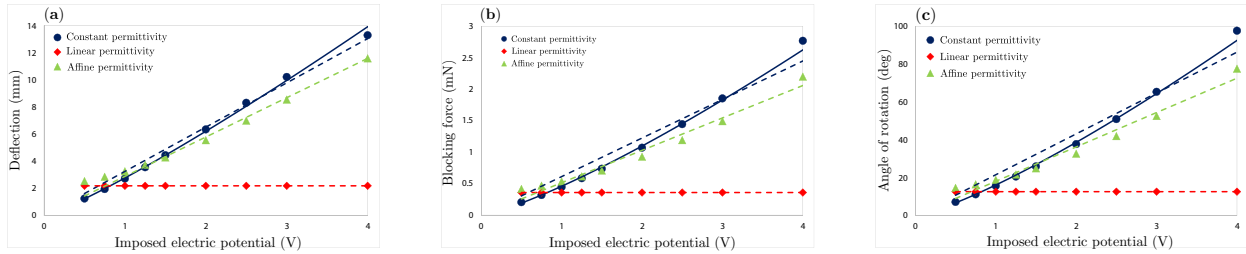


Figure 12. Influence of the electric potential: (a) on the deflection; (b) on the blocking force; (c) on the angle of rotation (same colours marks and curves as in figure 9).

cisely, in the constant case, the curve that best fits our numerical results is a power law of exponent 1.16 (figure 12); this curve can hardly be distinguished from an experimental linear curve (Tixier & Pouget 2018). The blocking force and the angle of rotation follow approximately the same trend (good correlation with a linear law and with a power law of exponent 1.26). This result is in good agreement with Hasani et al. (2019) experimental data, which can be well fitted by a power law of exponent 1.5. In the linear case, the moment is independent of the imposed potential for $\varphi_0 \gtrsim 1$, as well as the deflection, the blocking force and the angle of rotation, which does not correspond to the experimental observations. In the affine case, the correlations with a linear law and with a power law are wrong for all the quantities. The variation of the different quantities with the imposed electric potential is thus discriminating for the permittivity model: only a constant permittivity gives results compatible with the experimental studies.

We can evaluate the average permittivity of the strip by analogy with a capacitor of thickness e and surface Ll subject to a potential difference φ_0 . We saw that the cations accumulate near the negative electrode over a thickness of $e' \ll e$, and that there was a similar thickness area without cations near the positive electrode. The electric charge density is about $\rho Z^+ = FC_{moy}(B_1 - 1)$ near the positive electrode and $\rho Z^- = -FC_{moy}$ near the negative one. The capacitive charge Q can therefore be estimated by

$$Q = (\rho Z^+ - \rho Z^-)\phi_4 l L e' = FC_{moy}\phi_4 l L e' B_1. \quad (55)$$

The permittivity is then worth

$$\varepsilon = \frac{Qe}{Ll\varphi_0} = \frac{FC_{moy}\phi_4 e e'}{\varphi_0} B_1. \quad (56)$$

In the case of constant permittivity, $B_1 = A_2$ hence $\varepsilon \sim 4 \cdot 10^{-3} - 4 \cdot 10^{-2}$. In the case of a linear or affine permittivity, $B_1 \simeq 2$ and $\varepsilon \sim 10^{-2}$. These values are consistent with the permittivity values derived from capacity measurements published in the literature (Nemat-Nasser 2002, Farinholt & Leo 2004).

The hydrated IPMC can be considered as a five-layer capacitor: the electrodes of thicknesses e_1 and e_5 , the central area of thickness e_3 very large compared to the previous thicknesses and of zero electric charge, and two very thin zones of the polymer of respective thicknesses e_2 and e_4 in the vicinity of the positive and negative electrodes. Each element has a permittivity ε_i and a capacity $C_i = \varepsilon_i \frac{L}{e_i}$, and the five elements are in series. The permittivity of a material being closely related to its conductivity, so here to the cation concentration, $\varepsilon_1 = \varepsilon_5 \gg \varepsilon_2 \gg \varepsilon_3 \gtrsim \varepsilon_4$. In addition e_3 is much greater than e_1, e_2, e_4 and e_5 . We deduce

$$\varepsilon = \frac{e}{\frac{e_1 + e_5}{\varepsilon_1} + \frac{e_2}{\varepsilon_2} + \frac{e_3}{\varepsilon_3} + \frac{e_4}{\varepsilon_4}} \simeq \varepsilon_3,$$

where e denotes the total thickness. The overall permittivity of the strip subject to an electric field is therefore very close to the permittivity of the central part, which is that of the hydrated polymer without electric field. Our average permittivity values range from $5 \cdot 10^{-7} F m^{-1}$ to $10^{-4} F m^{-1}$ depending on the permittivity model and are thus compatible with the permittivity values measured by Deng & Mauritz (1992) and Wang et al. (2014), which range from $10^{-7} F m^{-1}$ to $5 \cdot 10^{-3} F m^{-1}$.

5. Conclusion

We studied the flexion of an ionic polymer strip using a model based on the thermomechanical of continuous media that we had previously developed. The strip, clamped at one of its ends, is subject to a continuous potential difference applied between its two faces (static case). The other end is either free or blocked by a shear force. The mechanical quantities (deflection, blocking force and angle of rotation) were determined using a beam model in large displacements. The material chosen to perform the simulations is Nafion[®] Li⁺. Three models of permittivity (constant, linear and affine functions of cation concentration) are examined. The permittivity values we used are in good agreement with dielectric spectroscopy and

electrical impedance measurements, but significantly lower than those deduced from capacity measurements. The resolution of the equations of our model enabled us to plot the cation concentration, pressure, electric potential and displacement profiles over the thickness of the strip. These quantities are almost constant in the central part, but vary drastically in the vicinity of the electrodes, which is characteristic of a conductive material. The scaling laws obtained for the deflection and the blocking force are in good agreement with the experimental data published in the literature: in particular, the deflection varies as the square of the strip length and is inversely proportional to the square of its thickness; the blocking force is proportional to the width and the thickness and it is inversely proportional to the length. The variation of the mechanical quantities with the imposed electric potential depends on the chosen permittivity model; only the constant permittivity model provides results compatible with the experimental data and will therefore be retained for further works. We now plan to apply our model to other materials close to the Nafion[®] and to study other configurations such as a strip clamped at its two ends.

Notations

$k = 1, 2, 3, 4, i$ subscripts respectively represent cations, solvent, solid, solution (water and cations) and interface; quantities without subscript refer to the whole material. Superscript ⁰ denotes a local quantity; the lack of superscript indicates average quantity at the macroscopic scale. Superscript ^T indicates the transpose of a second-rank tensor. Overlined letters denote dimensionless quantities.

A_i, B_i : dimensionless constants;

C, C_{moy} : cations molar concentrations (relative to the liquid phase);

D : mass diffusion coefficient of the cations in the liquid phase;

\vec{D} : electric displacement field;

e : half-thickness of the strip;

E, G, λ : Young's and shear modulus, first Lamé constant;

\vec{E} : electric field;

$F = 96487 \text{ C mol}^{-1}$: Faraday's constant ;

$\vec{F}^p (\vec{F}_s^p)$: blocking force on large (small) displacements;

\vec{I} : current density vector;

I^p : moment of inertia;

K : intrinsic permeability of the solid phase;

l : half-width of the strip;

L : length of the strip;

M_k : molar mass of component k ;

M_{eq} : equivalent weight (weight of polymer per mole of sulfonate groups);

$\vec{M}^p (\vec{M}_A^p)$: bending moment;

$\vec{n} (\vec{n})$: normal vector (coordinate) to the beam;

p : pressure;

\vec{p}^p : distributed electric force

\vec{Q} : heat flux;

$R = 8,314 \text{ J K}^{-1}$: gaz constant;

R^p : radius of curvature of the beam;

$s (\bar{s})$: curvilinear abscissa along the beam at rest (deformed)

S : entropy density;

T : absolute temperature;

\vec{u} : displacement vector;

U : internal energy density;

v_k : partial molar volume of component k (relative to the liquid phase);

$\vec{V} (\vec{V}_k)$: velocity;

$w (w_s)$: deflection of the beam on large (small) displacements;

$Z (Z_k)$: total electric charge per unit of mass;

$\varepsilon (\varepsilon^0, \varepsilon_{moy})$: permittivity (average permittivity);

$\underline{\varepsilon}$: strain tensor;

η_2 : dynamic viscosity of water;

θ : angle of rotation of a beam cross section;

λ_v, μ_v : viscoelastic coefficients;

μ_k : mass chemical potential;

$\rho (\rho_k)$: mass density relative to the volume of the whole material;

ρ_k^0 : mass density relative to the volume of the phase;

$\underline{\sigma} (\underline{\sigma}_k), \underline{\sigma}^e$: stress tensor, equilibrium stress tensor;

ϕ_k : volume fraction of phase k ;

$\varphi (\varphi_0)$: electric potential (imposed electric potential);

References

- Aureli, M. and Prince, C. and Porfiri, M. and Peterson, S.D. 2010 *Smart Materials and Structures* **19**, 015003.
- Bahramzadeh, Y. and Shahinpoor, M. 2014 *Soft Robotics* **1**(1), 38–52.
- Bakhtiarpour, P. and Parvizi, A. and Müller, M. and Shahinpoor, M. and Marti, O. and Amirkhani, M. 2016 *Smart Materials and Structures* **25**, 015008 doi:10.1088/0964-1726/25/1/015008.
- Bar-Cohen, Y. 2005 *WIT Transactions on State of the Art in Science and Engineering* **20**, 66–81.
- Barclay Satterfield, M. and Benziger, J. B. 2009 *J. Polym. Sci. Pol. Phys.* **47**(1), 11–24.

- Bauer, F. and Denneler, S. and Willert-Porada, M. 2005 *Journal of Polymer Science part B : Polymer Physics* **43**(7), 786–795.
- Biot, M.A. 1977 *International Journal of Solids and Structures* **13**, 579–597.
- Bluhm, J. and Serdas, S. and Schröder, J. 2016 *Archive of Applied Mechanics* **86**, 3–19.
- Brunetto, P. and Fortuna, L. and Graziani, L. and Strazzeri, S. 2008 *Smart Materials and Structures* **17**, 025029.
- Cappadonia, M. and Erning, J. and Stimming, U. 1994 *Journal of Electroanalytical Chemistry* **376**(1), 189–193.
- Cha, Y. and Shen, L. and Porfiri M. 2013 *Smart Materials and Structures* **22**, 055027.
- Chabé, J. 2008 Etude des interactions moléculaires polymère-eau lors de l'hydratation de la membrane Nafion, électrolyte de référence de la pile à combustible. PhD thesis Université Joseph Fourier Grenoble I http://tel.archives-ouvertes.fr/docs/00/28/59/99/PDF/THESE_JCS.pdf.
- Chen, Z. 2017 *Robotics and Biomimetics* **4**(24), <https://doi.org/10.1186/s40638-017-0081-3>
- Chikhaoui, M.T. and Benouhiba, A. and Rougeot, P. and Rabenorosoa, K. and Ouisse, M. and Andreff, N. 2018 *Annals of Biomedical Engineering* **16**(10), 1511–1521. <https://doi.org/10.1007/s10439-018-2038-2>.
- Collette, F. 2008 Vieillessement hygrothermique du Nafion. PhD Thesis Ecole Nationale Supérieure des Arts et Métiers http://tel.archives-ouvertes.fr/docs/00/35/48/47/PDF/These_Floraine_COLLETTE_27112008.pdf.
- Coussy, O. 1995 *Mechanics of porous continua*. Wiley Chichester.
- de Groot, S. R. and Mazur, P. 1962 *Non-equilibrium thermodynamics*. North-Holland publishing company Amsterdam
- Deng, Z.D. and Mauritz, K.A. 1992 *Macromolecules* **25**(10), 2739–2745.
- Deole, U. and Lumia, R. and Shahinpoor, M. and Bermudez, M. 2008 *Journal of Micro-Nano Mechatronics* **4**, 95–102.
- Fang, B.K. and Ju, M.S. and Lin, C.C.K. 2007 *Sensors and Actuators A* **137**(2), 321–329.
- Farinholt, K. and Leo, D.J. 2004 *Mechanics of Materials* **36**(5), 421–433.
- Farinholt, K. and Pedrazas, N.A. and Schluneker, D.M. and Burt, D.W. and Farrar, C.R. 2009 *Journal of Intelligent Material Systems and Structures* **20**(5), 633–642.
- Festin, N. and Plesse, C. and Pirim, P. and Chevrot, C. and Vidal, F. 2014 *Sensors and Actuators B: Chemical* **193**, 82–88.
- Gierke, T.D. and Munn, G.E. and Wilson, F.C. 1981 *Journal of Polymer Science : Polymer Physics Edition* **19**(11), 1687–1704.
- Hasani, M. and Alaei, A. and Mousavi, M. S. S. and Esmaili, E. and Kolahdouz, M. and Naeini, V. F. and Masnadi-Shirazi, M. 2019 *Journal of Micromechanics and Microengineering* **29**, 085008 <https://doi.org/10.1088/1361-6439/ab272c>.
- He, Qingsong and Yu, Min and Song, Linlin and Ding, Haitao and Zhang, Xiaoqing and Dai, Zhendong 2011 *Journal of Bionic Engineering* **8**, 77–85.
- Ishii, M. and Hibiki, T. 2006 *Thermo-fluid dynamics of two-phase flow*. Springer New-York.
- Jean-Mistral, C. and Basrou, S. and Chaillout, J.J. 2010 *Smart Materials and Structures* **19**, 085012.
- Jo, C. and Pugal, D. and Oh, I. and Kim, K.J. and Asaka, K. 2013 *Progress in Polymer Science* **38**, 1037–1066
- Lakshminarayanaiah, N. 1969 *Transport Phenomena in Membranes*. Academic Press New-York.
- Lin, J. and Liu, Y. and Zhang, Q.M. 2012 *Macromolecules* **45**(4), 2050–2056.
- Matysek, M. and Lotz, P. and Schlaak H.F. 2009 *Proc. SPIE 7287, Electroactive Polymer Actuators and Devices (EAPAD)* **7287**, 72871D doi: 10.1117/12.819217.
- Mojarrad, M. and Shahinpoor, M. 1997 *Proc. SPIE* **3042**, 52–60.
- Nardinocchi, P. and Pezzulla, M. and Placidi, L. 2011 *Journal of Intelligent Material Systems and Structures* **22**(16), 1887–1897.
- Nemat-Nasser, S. 2002 *Journal of Applied Physics* **92**(5), 2899–2915.
- Nemat-Nasser, S. and Li, J. 2000 *Journal of Applied Physics* **87**(7), 3321–3331.
- Newbury, K.M. 2002 Characterization, modeling and control of ionic-polymer transducers. PhD thesis Faculty of the Virginia Polytechnic Institute and State University Blacksburg, Virginia.
- Newbury, K.M. and Leo, D.J. 2002 *Journal of Intelligent Material Systems and Structures* **13**(1), 51–60.
- Newbury, K.M. and Leo, D.J. 2003 *Journal of Intelligent Material Systems and Structures* **14**(6), 343–357.
- Nguyen, N.T. and Dobashi, Y. and Soyer, C. and Plesse, C. and Nguyen, G.T.M. and Vidal, F. and Cattan, E. and Grondel, S. and Madden, J.D.W. 2018 *Smart Materials and Structures* **27**, 115032.
- Park, I. and Kim, S.M. and Pugal, D. and Huang, L. and Tam-Chang, S.W. and Kim K.J. 2010 *Applied Physics Letters* **96**(4), 043301.
- Pugal, D. and Jung, K. and Aabloob, A. and Kim, K.J. 2010 *Polymer International* **59**, 279–289.
- Shahinpoor, M. 1999 *Proc. of SPIE* **3669**, 109–121.
- Shahinpoor, M. and Bar-Cohen, Y. and Simpson, J.O. and Smith, J. 1998 *Smart Materials and Structures* **7**(6), R15–R30.
- Shahinpoor, M. and Kim, K.J. 2001 *Smart Materials and Structures* **10**(4), 819–833.
- Silberstein, M. N. and Boyce, M. C. 2010 *J. Power Sources* **195**(17), 5692–5706.
- Tiwari, R. and Kim, K. J. and Kim, S. M. 2008 *Smart Structures and Systems* **4**(5), 549. DOI: 10.12989/sss.2008.4.5.549.
- Tixier, M. and Pouget, J. 2014 *Continuum Mechanics and Thermodynamics* **26**(4), 465–481.
- Tixier, M. and Pouget, J. 2016 *Continuum Mechanics and Thermodynamics* **28**(4), 1071–1091.
- Tixier, M. and Pouget, J. 2018 *Chapter 39: Modelling of an Ionic Electroactive Polymer by the Thermodynamics of Linear Irreversible Processes in Generalized Models and Non Classical Mechanical Approaches in Complex Materials* Springer Berlin.
- Vokoun, D. and Qingsong, He and Heller, L. and Min, Y. and Zhen, D.D. 2015 *Journal of Bionic Engineering* **12**(1), 142–151.
- Wallmersperger, T. and Horstmann, A. and Kröplin, B. and Leo, D.J. 2009 *Journal of Intelligent Material Systems and Structures* **20**, 741–750.
- Wang, Y. and Zhu, Z. and Chen, H. and Luo, B. and Chang, L. and Wang, Y. and Li, D. 2014 *Smart Materials and Structures* **23**(125015). doi:10.1088/0964-1726/23/12/125015.